Computational Materials Science 72 (2013) 32–37

Contents lists available at SciVerse ScienceDirect

Computational Materials Science

journal homepage: www.elsevier.com/locate/commatsci

First principle study of Ce doping and related complexes in GaN

Qianqian Li, Qiuyan Hao, Ying Li *, Guodong Liu

School of Materials Science and Engineering, Hebei University of Technology, Tianjin 300130, China

ARTICLE INFO

Article history:
Received 13 September 2012
Received in revised form 20 January 2013
Accepted 23 January 2013
Available online 6 March 2013

Keywords:
Ce-doped GaN
Formation energy
Electronic structure
Optical properties

ABSTRACT

Using LDA+*U* method, we investigate the formation energy, electronic structure, and optical properties of rare earth Ce isolated substitutional and related complexes with neighboring N or Ga vacancies in wurtzite GaN. Our results reveal that Ce_{Ga} introduces a localized defect level contributed by Ce-4*f* states in the band gap. The defect complexes $Ce_{Ga}V_N$ and $Ce_{Ga}V_{Ga}$ introduce the shallow donor levels and acceptor levels, respectively. The doping of Ce in GaN gives rise to spin polarization. Both the substitutional Ce dopants and defect complexes can lead to new peaks from defect levels electronic transitions in the low energy regions of imaginary dielectric function and absorption spectrum.

1. Introduction

Over the past decades, the luminescent properties of rare-earth (RE) ions doping in semiconductors have received wide attention because RE-doped semiconductors can emit light from the RE 4*f*-shell by means of electrical injection. In 1989, Favennec et al. [1] demonstrated that the thermal quenching of erbium doped semiconductors decreases with increasing band gap of the host material. Among the wide band gap semiconductors, GaN can be an ideal host candidate for RE ions because of its high field transport characteristics and incorporating with the RE ions very well. Recently, RE-doped GaN have attracted considerable interest due to their potential applications in optoelectronic devices [2–5]. For instance, RE-doped GaN samples have been exploited for the realization of flat panel displays (FPDs), high contrast thick dielectric electroluminescent (TDEL) display devices and thin film electroluminescent (TFEL) display devices [6]. GaN:RE based devices would become the standard for full color displays as well as optical communications such as the area of optical fibers in the future.

It was reported experimentally that strong blue, green and red emission can be observed in amorphous GaN thin films doped with Ce^{3+}, Tb^{3+} and Eu^{3+} ions [7], respectively, at room temperature. In addition, Tm-doped GaN can exhibit the blue light at 477 nm and infrared (IR) light at 804 nm [8]. Band gap narrowing and a red shift of absorption edge were observed in *p*-GaN implanted with Ce [9,10]. Theoretically, Sanna et al. [11], using LDA+*U* method, studied RE (Eu, Er, and Tm) related defect pairs in GaN and concluded that RE elements show a strong preference for the Ga-lattice site either as isolated substitutional or complexes with intrinsic defects. Svane et al. [12] used a self-interaction corrected (SIC) approach beyond LDA–DFT to investigate the electronic structure of substitutional rare-earth defects in cubic GaAs and GaN. Among all RE elements, Cerium has the largest trivalent ionic radius and has only one 4*f* electron, which is a unique element. However, for the optical properties of Ce-doped GaN there are relatively little experimental reports and no theoretical study is found so far.

In this paper, we investigate the formation energy, electronic structures and optical properties of substitutional Ce and its complexes with intrinsic defects in wurtzite GaN by first-principle method based on density functional theory. We first calculate the crystal parameters and bond lengths of five defect configurations, i.e. two intrinsic defects and three impurities defects. Then the formation energies of these defect configurations in different charge states are studied. Finally, we analyze the electronic structures and optical properties of three impurities defects in Ce-doped GaN.

2. Computational details

In this work, all calculations for intrinsic defects and Ce-related defect complexes in wurtzite GaN are performed with the Vienna ab initio simulation package (VASP) using the pseudopotential plane-wave scheme [13]. The interactions between ions and electrons are described by the projector augmented wave (PAW) method developed by Blöchl [14,15]. The cutoff energy of the plane wave basis is 500 eV, and the Brillouin-zone integration is performed by $5 \times 5 \times 3$ Mokhorst–Pack special *k*-points. All atoms are fully relaxed with the total energy change less than 10^{-5} eV and the force on each ion less than 0.03 eV/Å. The Ga $3d^{10}4s^24p^1$, N $2s^22p^3$ and Ce $4f^15s^25p^65d^16s^2$ are considered as valence

* Corresponding author. Tel.: +86 22 6020 4765; fax: +86 22 6020 4129.
E-mail address: liyingphy@126.com (Y. Li).

0927-0256/$ - see front matter
http://dx.doi.org/10.1016/j.commatsci.2013.01.029

electrons. The strong correlation effect of the Ce 4*f* electrons is treated by the local spin density approximation with Hubbard-U corrections (LSDA+*U*) with the values of $U = 7.47$ eV and $J = 0.99$ eV taken from Ref. [16]. We also calculate the partial Ce 4*f* electrons spin-polarized density of states with values of $U - J$ (U_{eff}) ranging from 0 to 8.01 eV.

To simulate the defect properties, a $3 \times 3 \times 2$ GaN supercell containing 72 atoms ($Ga_{36}N_{36}$) is employed. We substitute one Ce for one Ga atom as isolated substitutional, i.e., $Ga_{35}CeN_{36}$ (Ce_{Ga}) as illustrated in Fig. 1a, corresponding to a 2.78% Ce doping concentration. We produce two defect complexes by replacing one Ga atom with one Ce atom and simultaneously removing one neighboring N or Ga atom, i.e., $Ga_{35}CeN_{35}$ ($Ce_{Ga}V_N$) and $Ga_{34}CeN_{36}$ ($Ce_{Ga}V_{Ga}$), as illustrated in Fig. 1b and c. Note that only the Ce substitutional Ga-site is considered here because the RE_{Ga} has been both experimentally and theoretically found to be the most stable configuration in all states [17,18]. In this paper we mainly focus our investigation on three types of Ce-related defects in GaN, i.e., Ce_{Ga}(GaN:Ce), $Ce_{Ga}V_N$(GaN:Ce + V_N) and $Ce_{Ga}V_{Ga}$(GaN:Ce + V_{Ga}), and also calculate the pure GaN and single N or Ga vacancy for comparison.

3. Results and discussions

3.1. Crystal parameters

In Table 1, we list the calculated lattice constants and local Ce–N bond lengths around defects for different Ce-related defects in GaN. Structure parameters of pure GaN are also given for comparison. Our calculated lattice constants and bond lengths in pure GaN are slightly larger than the experiment data [19], which is in good agreement with other theoretical works [20,21].

For GaN:Ce, three equal Ce–N bond lengths and one Ce–N bond length in *c*-axis are 2.234 Å and 2.273 Å, which expand about 13.9% and 15.4% compared with the pure GaN, respectively. The expansion of Ce-doped GaN crystal structure is due to the ionic radius of Ce (1.03 Å) larger than that of Ga (0.62 Å). For GaN:Ce + V_N, there exist two defect configurations with C_{1h} and C_{3v} symmetry which are almost energetically degenerate [11]. Here we discuss the ideal axial configuration with the C_{3v} symmetry created by substituting a Ce for a Ga site and removing the nearest N ligand along the *c*-axis, as shown in Fig. 1b. The lattice constants are found to be slightly smaller than those of GaN:Ce and three equal bond lengths are larger compared with GaN:Ce due to the Ce impurity moving toward the N vacancy. For GaN:Ce + V_{Ga}, removing one of 12*s* neighbors Ga atoms of the isolated Ce substitutional can originate three different $Ce_{Ga}V_{Ga}$ complexes, having the C_{1h} or C_1 symmetry but almost degenerate energies, as reported in Ref. [11]. We calculate one defect complex with the C_{1h} symmetry, as shown in Fig. 1c. The calculated lattice constants *a* and *b* become unequal, and the bond length of Ce–N in *c*-axis slightly decreases compared with the GaN:Ce.

Table 1
Calculated structural parameters for GaN, GaN:Ce, GaN:Ce + V_N and GaN:Ce + V_{Ga}. The a, b, c are lattice constants. Bond length is the length of Ga–N or local Ce–N bonds around defects. All numbers are in units of Å.

		a (*b*)	*c*	Bond length
GaN	This work	3.210	5.232	1.962, 1.969
	Other's work	3.203[a]	5.217	–
		3.209[b]	5.219	–
	Experiment	3.189[c]	5.185	1.952, 1.944
GaN:Ce		3.236	5.266	2.234, 2.273
GaN:Ce + VN		3.221	5.247	2.239, –
GaN:Ce + VGa		3.229(3.219)	5.263	2.332/2.192, 2.073

[a] Ref. [20].
[b] Ref. [21].
[c] Ref. [19].

Theoretically, which type of defect in the three Ce dopant defects is most likely to form depends on its formation energy. The formation energy of a defect or impurity *X* in charge state *q* is usually defined as [22]

$$E_f[X^q] = E_{\text{tot}}[X^q] - E_{\text{tot}}[\text{GaN, bulk}] - \Sigma n_i \mu_i + q[E_F + E_v + \Delta V],$$

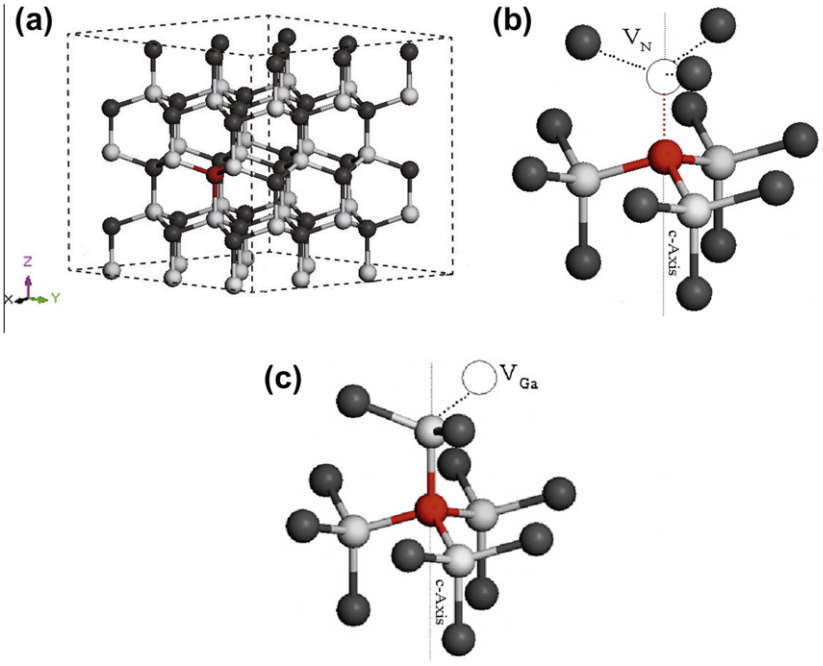

Fig. 1. Three defect configurations in Ce doped hexagonal GaN: (a) the Ce_{Ga} substitutional in hexagonal GaN supercell ($3 \times 3 \times 2$) containing 72 atoms, (b) defect pairs ($Ce_{Ga}V_N$) formed by Ce_{Ga} substitutional and V_N in hexagonal GaN, and (c) defect pairs ($Ce_{Ga}V_{Ga}$) formed by Ce_{Ga} substitutional and V_{Ga} in hexagonal GaN. Ga atoms are black, nitrogen atoms white, and Ce atom red. (For interpretation of the references to color in this figure legend, the reader is referred to the web version of this article.)

where $E_f[X^q]$ is the total energy of the supercell calculated with one impurity or defect X, and E_{tot}[GaN, bulk] is the total energy for the pure GaN. n_i indicates the number of atoms of type i (host atoms or impurity atoms) that have been added to ($n_i > 0$) or removed from ($n_i < 0$) the supercell when the defect or impurity is created, and the u_i are the corresponding chemical potentials of these species. E_F is the Fermi level, referenced to the valence-band maximum (VBM) E_v in GaN. ΔV is the alignment of the averaged electrostatic potential in our defect supercell with that in the bulk. For N-rich condition, excess N is assumed to exist as N_2 gas, i.e. $\mu_N = \frac{1}{2}E(N_2), \mu_{Ga} = E(GaN) - \mu_N$, while excess rare earth is assumed in the form of the rocksalt structure, i.e. $\mu_{Ce} = E(CeN) - \mu_N$.

To give a reasonable description of both defect levels and band edges, we first carry out a calculation on energy band gap from electron addition and removal. According to $E^-[R(-)] + E^+[R(+)] - 2E^0[R(0)]$ [23], our calculated band gap is 3.25 eV, in acceptable agreement with the experiment value of 3.39 eV. Fig. 2 shows the formation energies as a function of Fermi level for Ce dopant defects Ce_{Ga}, $Ce_{Ga}V_N$ and $Ce_{Ga}V_{Ga}$ and also V_N and V_{Ga} for comparison in different charge states. We see that V_N behaves as donors in GaN, and the (3+/+) charge transition level occurs at 0.81 eV, a little higher than 0.59 eV reported in Ref. [22]. The V_{Ga} acts as a triple acceptor, and the transition levels (0/−), (−/2−) and (2−/3−) are at 0.21, 0.72 and 1.06 eV above the VBM, respectively, which are well consistent with results reported in Ref. [22]. The V_N has the low formation energy under *p*-type condition while the V_{Ga} has the low formation energy under *n*-type condition.

In the case of Ce_{Ga}, the (+/0) and (0/−) transition levels occur at 0.82 eV and 2.39 eV above the VBM, respectively. In *p*-type GaN, the Ce_{Ga} prefers to be positive charge while in *n*-type GaN the Ce_{Ga} prefers to be negative charge. The thermodynamic transition levels are deep levels, which are not easy to contribute to the photoluminescence observed in experiment [7]. For defect complexes $Ce_{Ga}V_N$, the binding energy of the Ce impurity and the nitrogen vacancy under neutral states is 0.98 eV. One charge transition level (0/−) is found at 2.95 eV over the valence band. This is a shallow level and can play a role in the photoluminescence. The other charge transition level (+/0) is at 1.65 eV. For another defect pair $Ce_{Ga}V_{Ga}$, the binding energy of the Ce impurity and the Ga vacancy under neutral states is 1.59 eV larger than that of $Ce_{Ga}V_N$. Three charge transition levels (0/−), (−/2−) and (2−/3−) are located at 0.35, 1.02 and 1.42 eV above the VBM, respectively. By comparing with the two defect complexes, we find that under N-rich conditions $Ce_{Ga}V_N$ has a lower formation energy in *p*-type GaN while $Ce_{Ga}V_{Ga}$ is energetically favored in *n*-type GaN. In addition, it is found that the charge transition levels in Ce-doped GaN are very similar with those in RE (Eu, Er, and Tm) doped GaN [11].

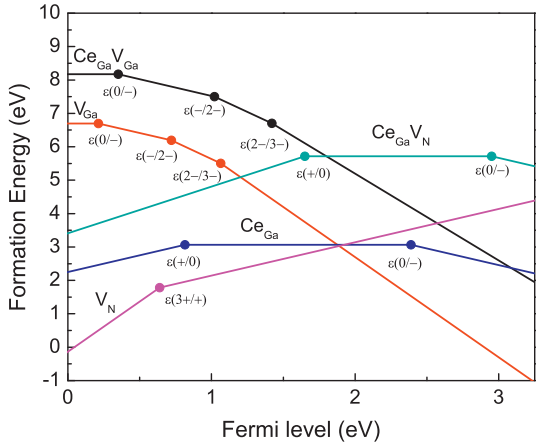

Fig. 2. Formation energy as a function of the Fermi energy for the isolated Ce_{Ga}, $Ce_{Ga}V_N$ pairs, $Ce_{Ga}V_{Ga}$ pair, and native point defects V_N and V_{Ga} in GaN. N-rich conditions are assumed. The zero of Fermi level corresponds to the top of the valence band.

3.2. Electronic structure

In Figs. 3 and 4, we present the electronic band structure and the total density of states (DOSs) and partial density of states (PDOSs) for GaN:Ce, GaN:Ce + V_N and GaN:Ce + V_{Ga} and also GaN (primitive cell) for comparative purpose. Obviously, GaN is a direct gap semiconductor with the energy gap of 1.75 eV (Fig. 3a), which is much smaller than the experiment value of 3.39 eV because of the well-known underestimation of DFT calculations as reported in other work [24]. In contrast with GaN, GaN:Ce exhibits an indirect band gap of 1.48 eV with the conduction band minimum (CBM) at point Γ and the VBM at point H (Fig. 3b). The dopant Ce introduces an impurity level at 0.55 eV above the VBM within the energy gap, and the energy band shifts towards the low energy regions. This can be also seen clearly from Fig. 4a. The band gap narrowing of GaN:Ce makes the optical transition easy, which will help improve the optical performance of the GaN. For GaN:Ce + V_N (Fig. 3c), there appear two defect levels derived from the N vacancy at the bottom of conduction bands in both the majority and minority spin band structures while one impurity level is found to be in the majority spin band structure. For GaN:Ce + V_{Ga} (Fig. 3d), seven local levels derived from Ce arise at the bottom of the conduction band while there are three acceptor levels associated with the Ga vacancy above the valence band in the minority spin band structure.

According to the density of states shown in Fig. 4a, we see that in GaN:Ce the conduction band is primarily attributed to Ga-4*s*, Ga-4*p*, Ga-3*d*, N-2*p*, and Ce-4*f* states. The local Ce-4*f* states give rise to several relatively strong peaks at −0.08 eV (majority spin), 5.94 eV (majority spin) and 6.26 eV (minority spin). A small peak at −0.08 eV is also found in the majority spin N-2*p* states. In addition, the introduction of Ce impurity leads to the magnetic ordering and the magnetic moment of 1.00 μ_B induced mostly by Ce-4*f* and a little by N-2*p* states. Experimentally, weak ferromagnetism at high temperature is observed in 1% Ce doped GaN [25]. For GaN:Ce + V_N (Fig. 4b), the Fermi surface shifts slightly towards high energy regions compared to GaN:Ce due to the donor character of the V_N. The donor states near the CBM are determined by N-2*p* and Ga-4*p* states. The impurity state near the Fermi surface is contributed by Ce-4*f* and N-2*p* states, and the impurity state near the VBM is mainly determined by N-2*p* states. The Ce-4*f* states give rise to two strong peaks at 6.01 eV (majority spin) and 5.74 eV (minority spin) in the conduction band. The magnetic moment decreases to 0.67 μ_B. For GaN:Ce + V_{Ga} (Fig. 4c), the Fermi surface shifts towards low energy regions because of the acceptor character of V_{Ga}. There are strong peaks at 2.51 eV (majority spin), 1.41 eV and 2.83 eV (minority spin) mainly caused by Ce-4*f* state. The defect levels near the VBM are determined by N-2*p* state, and the impurity band below the CBM is attributed to N-2*p* and Ce-4*f* states. The spin magnetic moment is 2.00 μ_B.

Moreover, we also study the effect of the *U* value on the density of state of Ce 4*f* electrons by varying the U_{eff} parameter ranging from 0 to 8.01 eV. The DOS of spin-polarized Ce-4*f* electrons for five different values of U_{eff} are shown in Fig. 5. In the case of $U_{eff} = 0$, the localized 4*f*-related levels appear in the Fermi surface. As U_{eff} increases to 2.46 eV, the 4*f* electrons energy levels start to split. With the increasing U_{eff}, the empty 4*f* states shift slowly towards high energy regions, indicating that the 4*f* states do not undergo any hybridization with the host.

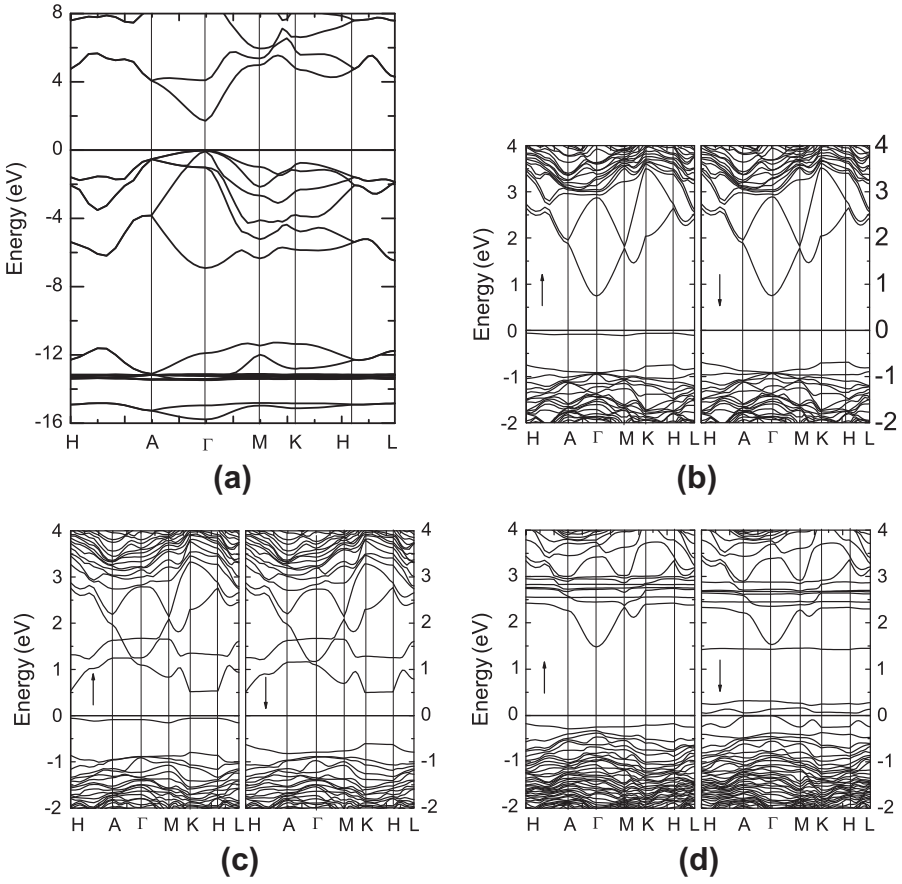

Fig. 3. Band structure of GaN and Ce-doped GaN defect configurations: (a) GaN (primitive cell), (b) GaN:Ce, (c) GaN:Ce + V_N, and (d) GaN:Ce + V_{Ga}. The Fermi level is set to be zero. Symbol ↑ means spin up and ↓ means spin down.

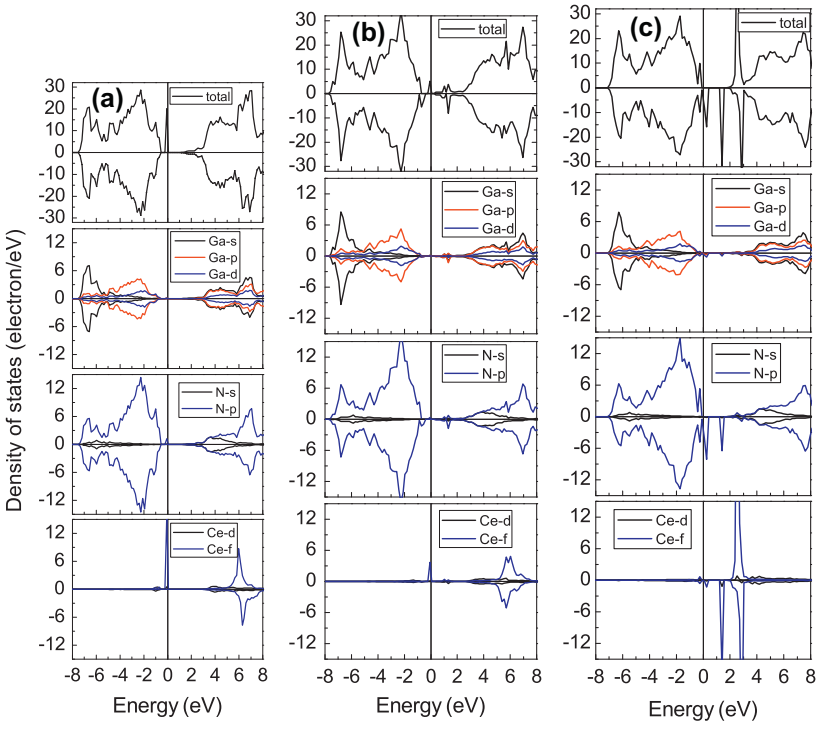

Fig. 4. Calculated total and partial density of states of (a) GaN:Ce, (b) GaN:Ce + V_N, and (c) GaN:Ce + V_{Ga}. The Fermi level is set to be zero, and the PDOS of Ce atom only show *d* and *f* states.

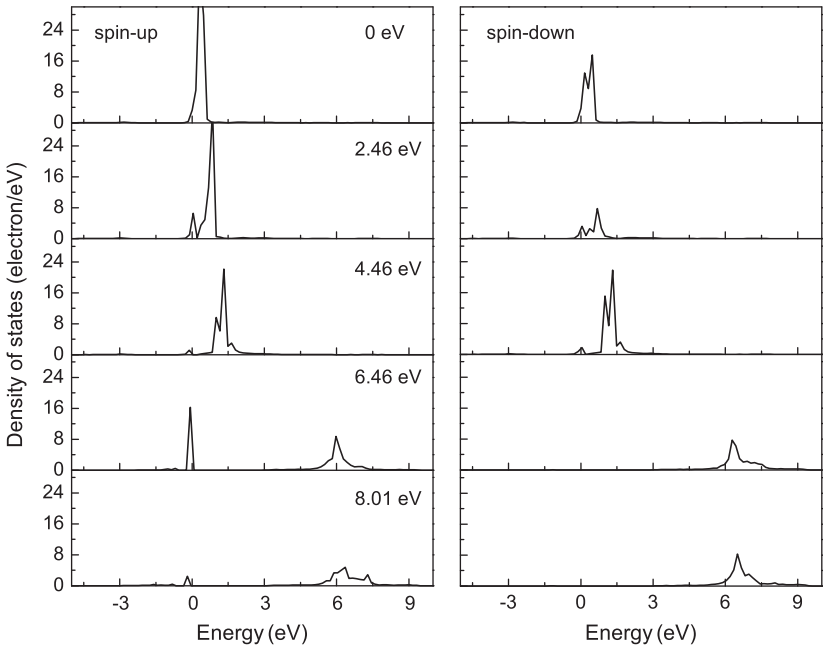

Fig. 5. The partial Ce-4*f* spin-polarized density of states for different values of U_{eff} ranging from 0 to 8.01 eV.

3.3. Optical properties

As for the optical spectra calculations, we use a summation over conduction band states to obtain the frequency-dependent dynamic dielectric function after the electronic ground state has been obtained. In the range of linear resonance, the solid optical resonance function often is described by the dielectric function. where $\varepsilon_1(\omega)$ and $\varepsilon_2(\omega)$ are the real and imaginary parts of the dielectric function, respectively. Other main optical spectra, such as the reflectivity $R(\omega)$, adsorption coefficient $I(\omega)$, energy-loss spectrum $L(\omega)$, and refractive index $n(\omega)$, can be obtained from the dynamic dielectric function $\varepsilon(\omega) = \varepsilon_1(\omega) + i\varepsilon_2(\omega)$ [26,27].

In Fig. 6, we show the imaginary part of dielectric function of GaN, GaN:Ce, GaN:Ce + V_N and GaN:Ce + V_{Ga} when the incident radiation has linear polarization along [001] and [100/010] directions, denoted as ε_2^{zz} and $\varepsilon_2^{xx}/\varepsilon_2^{yy}$. The imaginary part along the [100] direction has the same form as the [010] direction for GaN, GaN:Ce and GaN:Ce + V_N, i.e., $\varepsilon_2^{xx} = \varepsilon_2^{yy}$. For the pure GaN, the imaginary part of the dielectric function exhibits the first small peak at 2.62 eV and four main peaks at 6.34, 7.84, 8.89 and 10.94 eV for ε_2^{xx}. The first shoulder peak is attributed to the transition between VBM and CBM, and the second peak to the transition between N-2*p* and Ga-4*s* states, and the last two peaks to the transition between Ga-3*d* and N-2*s* states. For ε_2^{zz} there are five main peaks at 5.76, 7.84, 9.43, 10.56 and 11.22 eV. Our results are in good agreement with the recent GGA + PBE calculations performed by Zhang et al. [28]. The calculated static dielectric constant is 5.93 for ε_0^{xx} and 6.08 for ε_0^{zz}.

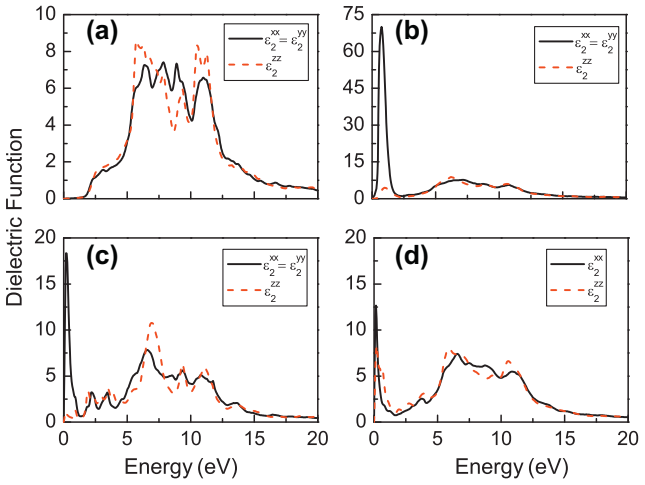

Fig. 6. Imaginary parts of dielectric function for (a) GaN, (b) GaN:Ce, (c) GaN:Ce + V_N, and (d) GaN:Ce + V_{Ga}.

For GaN:Ce, a very strong new peak appear at 0.74 eV for ε_2^{xx} and a relatively strong peak at 0.98 eV for ε_2^{zz}, as shown in Fig. 6b. These peaks should be ascribed to the transition between Ce-4*f* states and the conduction band. Other peaks at 7.14, 8.73 and 10.79 eV for ε_2^{xx} and at 6.23, 8.83 and 10.65 eV for ε_2^{zz} have a red shift compared with those peaks in pure GaN. This result is qualitatively similar with the experimental observations [10]. The calculated static dielectric constants increase to 84.50 for ε_0^{xx} and 10.85 for ε_0^{zz}. For the defect complex formed by Ce and neighboring N vacancy, i.e., GaN:Ce + V_N, one strong peak is observed at 0.19 eV for ε_2^{xx} and at 0.14 eV for ε_2^{zz}, which may be ascribed to the transitions between Ce-4*f* states and the conduction band, and two weak peaks at 2.24 and 3.43 eV for ε_2^{xx} and at 1.89 and 3.49 eV for ε_2^{zz} should originate from the transition from N-2*p* states near the VBM to the defect levels shown in Fig. 3c. Compared with GaN:Ce, four main peaks (6.58, 8.48, 9.34 and 10.79 eV) along [100] direction move slightly towards lower energy regions while the peaks (6.91, 9.35 and 11.08 eV) along [001] direction move slightly towards higher energy regions. The calculated static dielectric constants increase to 30.47 for ε_0^{xx} and 8.06 for ε_0^{zz}. For GaN:Ce + V_{Ga} (Fig. 6d), two new peaks appear at 0.15(0.20 eV) and 3.72(3.87) eV for $\varepsilon_2^{xx}(\varepsilon_2^{zz})$, respectively, which should be attributed to the transition between the valence band and N-2*p* state above the Fermi level or Ce-4*f* states in the band gap. The small peaks at 3.73 eV for ε_2^{xx} and at 1.97, 2.76 and 3.89 eV for ε_2^{zz} are associated with the transition of N-2*p* electrons from the valence band to the conduction band or the Ce-4*f* states within the band gap. Other peaks are at 6.58, 7.48, 8.71 and 10.87 eV for ε_2^{xx} and at 5.87, 9.38 and 10.52 eV for ε_2^{zz}. The calculated static dielectric constants increase to 25.03 for ε_0^{xx} and 19.96 for ε_0^{zz}.

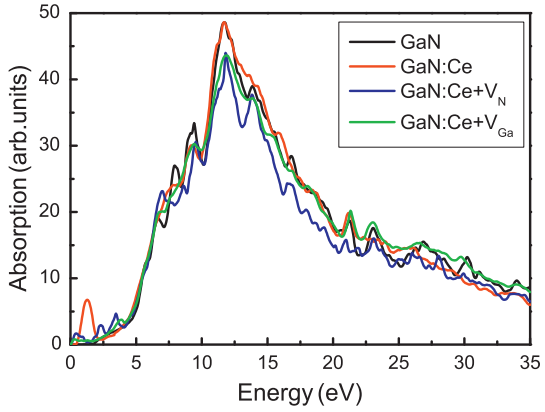

Fig. 7. Absorption coefficient for GaN (black solid line), GaN:Ce (red dash line), GaN:Ce + V_N (blue dot line), and GaN:Ce + V_{Ga} (green dash dot line). (For interpretation of the references to color in this figure legend, the reader is referred to the web version of this article.)

Furthermore, we calculate the absorption spectra of GaN doped with Ce. Fig. 7 shows the absorption coefficients as a function of energy along [100] direction for the pure GaN, GaN:Ce, GaN:Ce + V_N and GaN:Ce + V_{Ga}. In GaN, the absorption edge is found to be at 1.75 eV, corresponding to the calculated band gap, that is, the band-edge transitions. The main optical absorption peak is at 11.71 eV. In the case of GaN:Ce, a new peak appears at 1.27 eV, while the position and the intension of main peak remains unchanged. For GaN:Ce + V_N, three new peaks appear at 0.43, 2.32 and 3.47 eV while the main peak moves to 11.81 eV. For GaN:Ce + V_{Ga}, two new peaks are found at 0.31 and 3.86 eV and the main peak is at 11.94 eV. In contrast with the isolated Ce substitutional GaN, in two defect complexes the main absorption peaks shift slightly towards the higher energy and meantime the intensity of the peaks becomes weak. The origin of these peaks can also be explained by the peaks of the imaginary part $\varepsilon_2(\omega)$ shown in Fig. 6.

4. Conclusion

In summary, we have performed a detailed investigation of the structural parameters, electronic structure, and optical properties of the substitutional Ce and its complexes with vacancy defects in GaN, i.e., Ce_{Ga}, $Ce_{Ga}V_N$ and $Ce_{Ga}V_{Ga}$, by means of LDA+*U* calculation. The Ce_{Ga} substitution in GaN induces a small lattice distortion. The Ce_{Ga} introduces impurity levels derived from Ce-4*f* states in the band gap. The $Ce_{Ga}V_N$ and $Ce_{Ga}V_{Ga}$ defect pairs introduce new shallow levels as well as the impurity levels. The incorporation of nitrogen vacancy brings in donor levels near the CBM, whereas gallium vacancy introduces acceptor levels near VBM and impurity band from Ce-4*f* states near the bottom of conduction band. The incorporation of Ce impurity and vacancy can lead to the magnetic order and the magnetic moment of 1.00, 0.67 and 2.00 μ_B for GaN:Ce, GaN:Ce + V_N and GaN:Ce + V_{Ga}, respectively. Furthermore, according to the imaginary part of dielectric function and absorption spectra, we find that new peaks occur in the low energy regions after the introduction of Ce impurity and vacancy defects in GaN.

References

[1] P.N. Favennec, H. L'Haridon, M. Salvi, D. Moutonnet, Y.L. Guillou, Electron. Lett. 25 (1989) 718.
[2] A.J. Steckl, J.C. Heikenfeld, D. Lee, M.J. Garter, C.C. Baker, Y. Wang, R. Jones, IEEE J. Sel. Top. Quantum Electron. 8 (2002) 749.
[3] R. Jones, Opt. Mater. 28 (2006) 718–722.
[4] S. Chen, B. Dierre, W. Lee, T. Sekiguchi, S. Tomita, H. Kudo, K. Akimoto, Appl. Phys. Lett. 96 (2010) 181901.
[5] L. Jiang, X.L. Wang, H.L. Xiao, Z.G. Wang, C. Yang, M. Zhang, Appl. Phys. A 104 (2011) 429–432.
[6] A.J. Steckl, J.M. Zavada, Mater. Res. Bull. 24 (1999) 33.
[7] S.B. Aldabergenova, A. Osvet, G. Frank, H. Strunk, P. Taylor, A.A. Andreev, J. Non-Cryst. Solids 299–302 (2002) 709–713.
[8] K. Lorenz, E. Alves, U. Wahl, T. Monteir, S. Dalmasso, R. Martin, K. O'Donnell, R. Vianden, Mater. Sci. Eng. B 105 (2003) 97–100.
[9] A. Majid, J. Iqbal, A. Ali, J. Supercond. Nov. Magn. 24 (2011) 585–590.
[10] A. Majid, A. Ali, J. Phys. D: Appl. Phys. 42 (2009) 045412.
[11] S. Sanna, W.G. Schmidt, Th. Frauenheim, U. Gerstmann, Phys. Rev. B 80 (2009) 104120.
[12] A. Svane, N.E. Christensen, L. Petit, Z. Szotek, W.M. Temmerman, Phys. Rev. B 74 (2006) 165204.
[13] G. Kresse, J. Furthmüller, Phys. Rev. B 54 (1996) 11169.
[14] P. Blochl, Phys. Rev. B 50 (1994) 17953.
[15] G. Kresse, D. Joubert, Phys. Rev. B 59 (1999) 1758–1775.
[16] P. Larson, R.L. Lambrecht, Phys. Rev. B 75 (2007) 045114.
[17] H.J. Lozykowski, Phys. Rev. B 48 (1993) 17758.
[18] J.-S. Filhol, R. Jones, M.J. Shaw, P.R. Briddon, Appl. Phys. Lett. 84 (2004) 2841.
[19] P. Perlin, C. jauberthie-Carillon, J.P. Itie, A.S. Miguel, I. Grzegory, A. Polan, Phys. Rev. B 45 (1992) 83–89.
[20] S.T. Li, C.Y. Ouyang, Phys. Lett. A 336 (2005) 145–151.
[21] S. Li, C. Ouyang, J. Phys. Chem. Solids 70 (2009) 1223–1225.
[22] C.G.V. de Walle, J. Neugebauer, J. Appl. Phys. 95 (2004) 3851.
[23] S. Petit, R. Jones, M.J. Shaw, P.R. Briddon, B. Hourahine, T. Frauenheim, Phys. Rev. B 72 (2005) 073205.
[24] D.M. Simanovaskii, H.A. Tang, Appl. Phys. Lett. 91 (2003) 107601.
[25] K. Oganisian, P. Gluchowski, W. Strek, J. Rare Earth. 29 (2011) 1183–1187.
[26] H. Shi, M. Chu, P. Zhang, J. Nucl. Mater. 400 (2010) 151–156.
[27] M. Gajdos, K. Hummer, G. Kresse, J. Furthmuller, F. Bechstedt, Phys. Rev. B 73 (2006) 045112.
[28] S. Zhang, J. Shi, M. Zhang, M. Yang, J. Li, J. Phys. D: Appl. Phys. 44 (2011) 495304.